Session V, Wednesday, June 12

L16

PENTACENE GROWTH ON GRAPHENE BY IN SITU GISAXS AND GIWAXS

M. Jergel[1], P. Šiffalovič[1], P. Nádaždy[1], M. Bodík[1], E. Majková[1], M. Hodas[2], G. Duva[2], B. Reisz[2], F. Schreiber[2], O. Konovalov[3], W. Ohm[4]

[1]*Institute of Physics SAS, Dúbravská cesta 9, 845 11 Bratislava, Slovakia*
[2]*Institut für Angewandte Physik, Universität Tübingen, Tübingen 72076, Germany*
[3]*European Synchrotron Radiation Facility, Grenoble 38000, France*
[4]*Photon Science, Deutsches Elektronen-Synchrotron (DESY), Hamburg 22607, Germany*
matej.jergel@savba.sk

Keywords: pentacene growth, graphene, epitaxy, GISAXS, GIWAXS

Abstract

Thin films of small organic semiconducting molecules exhibit attractive optical and electronic properties depending on their molecular structure. Pentacene (PEN) molecules are known to form a lying-down phase on graphene that improves vertical electron transport and increases optical absorption and light harvesting. Here, we studied the mechanism of epitaxial PEN growth on graphene by in-situ GISAXS and GIWAXS techniques complemented by ex-situ AFM and polarized confocal Raman microscopy. Two principal stages of the growth were observed. First, nucleation and growth of PEN islands saturating in width and height at 1 monolayer thickness was observed. Later on, the islands continue to grow only along [100] direction of the PEN triclinic lattice adopting needle-like shape and copying hexagonal symmetry of the underlying graphene. The c* axis of PEN reciprocal lattice was found to be parallel to the [210] (armchair) direction of graphene and tilted by 18° with respect to the graphene surface. This suggests a 11° deviation of the PEN molecular chains from the graphene surface driven by the energy minimization in later stages of the islands growth.

Introduction

Thin films of small organic molecules are attractive for applications in light-emitting diodes, field-effect transistors or organic solar cells. The device performance critically depends on the molecular structure of the film which in turn depends on the substrate type. For the oxide surfaces such as SiO_2, the standing-up configuration is typical. It the last decade it has been shown that templating the substrate with two-dimensional materials, the lying-down configuration can be achieved. Hence, this approach offers a possibility to control the molecular orientation and properties of the small molecule organic films. Indeed, the lying-down configuration of pentacene (PEN) molecules after evaporation on graphene was observed. PEN is an archetypal type of small organic molecules that are frequently used in organic electronics and photovoltaics. In order to optimize preparation of PEN films with the lying-down configuration, a study of the mechanism of PEN growth on graphene is needed. This gave impetus for the work presented here.

Experimental details

The PEN molecules (Sigma-Aldrich) were thermally evaporated onto epitaxially grown graphene on hexagonal 4H-SiC(0001) substrate (Graphensic) in a deposition chamber that was equipped with a beryllium window for the in-situ grazing-incidence small-angle and wide-angle X-ray scattering (GISAXS, GIWAXS) experiments. The deposition rate was 1.38 Å/min. The in-situ GISAXS/GIWAXS measurements were done at the 0.1° angle of incidence at ID10 (9.25 keV) and PO3 (11.4 keV) synchrotron beamlines at ESRF Grenoble and DESY Hamburg, respectively. Two hybrid pixel detectors acquired simultaneously and repeatedly the GIWAXS and GISAXS patterns during the evaporation (Maxipix and Pilatus 300K at ESRF, Pilatus 300K and Pilatus 1M at DESY). The 60 s integration time used at ESRF was reduced to 100 ms at DESY to capture initial stages of the deposition. The ex-situ GIWAXS measurements were done on a custom-designed Nanostar X-ray setup (Bruker AXS) equipped with a Ga liquid-metal jet anode X-ray source Excillum (9.25 keV) at an angle of incidence of 0.15° with a Pilatus 300K detector. The AFM measurements (Bruker, Dimension Edge) were done in tapping mode and the polarized Raman measurements were performed on a confocal Raman microscope (Witec, Alpha300 R+).

Results and conclusions

The ex-situ GIWAXS pattern after the PEN film deposition shows 3 diffraction spots (Fig. 1a). The film thickness calculated from the deposition rate and time corresponds to that of 10 PEN monolayers (MLs) reported previously [1]. The diffraction spots have no symmetric counterparts on the opposite side of the pattern (not shown) suggesting a monocrystalline structure of the film. It is composed of PEN crystals forming needle-like islands that follow hexagonal symmetry of the underlying graphene (Fig. 1b). The hexagonal unit cell of epitaxially grown graphene on SiC is rotated by 30° from the SiC hexagonal unit cell. Supposing the triclinic PEN phase [2], the orientation of PEN lattice with respect to graphene can be thus found from the ex-situ GIWAXS pattern (Fig. 2a). The reciprocal c* axis of PEN crystal is aligned along [210] (armchair) graphene direction and tilted by 18° from the graphene surface. The crystallographic a axis of the PEN unit cell lies in the graphene plane. Taking into account the PEN molecule orientation in

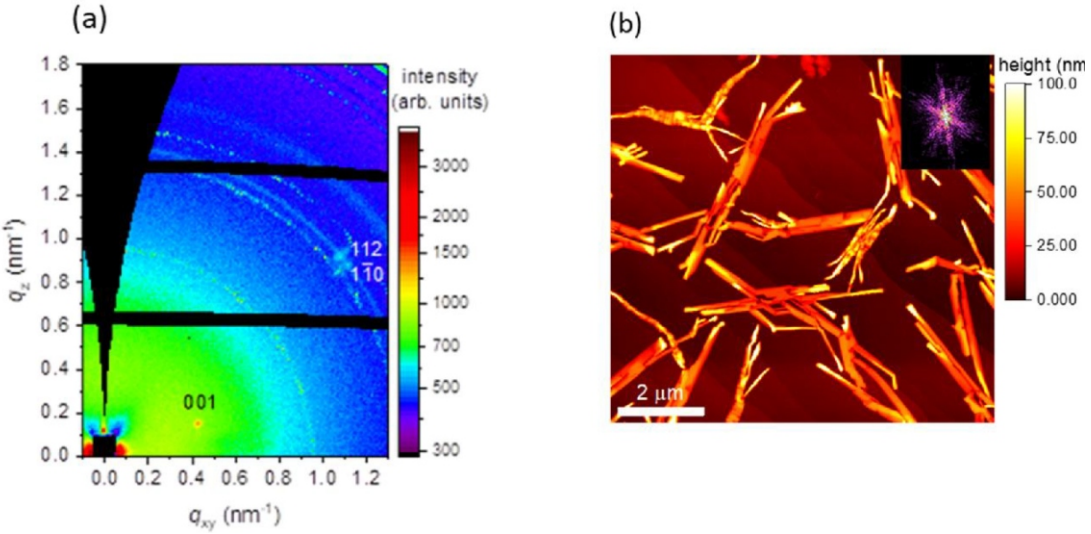

Figure 1. (a) GIWAXS pattern of PEN film and (b) its AFM image with Fourier transform in the inset.

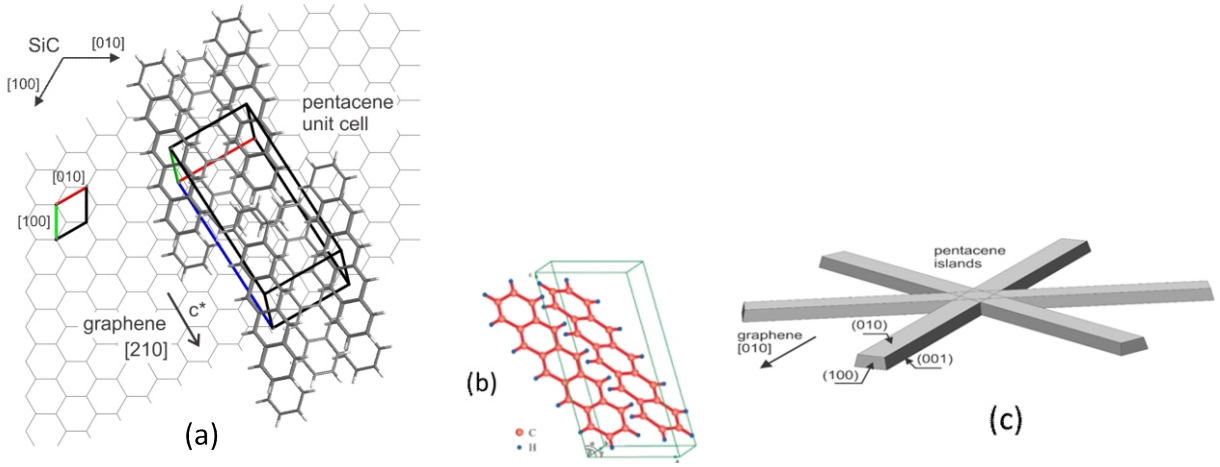

Figure 2. (a) Mutual orientation of PEN and graphene lattices. (b) PEN unit cell and (c) crystallographic orientation of PEN islands.

the unit cell (Fig. 2b), the long molecular axis does not follow the [100] (zigzag) graphene direction but is tilted by 11°. This is due to energy minimization in the presence of intermolecular interactions in three-dimensional PEN crystals. The blurred and 112 diffraction spots (Fig. 1a) originate from the crystals rotated by 120° and 300° (Fig. 2c). The ex-situ polarized confocal Raman microscopy revealed a uniform orientation of PEN molecular chains inside the islands, confirming thus their monocrystalline structure (Fig. 3).

The ex-situ GIWAXS pattern after the PEN film deposition shows 3 diffraction spots (Fig. 1a). The film thickness calculated from the deposition rate and time corresponds to that of 10 PEN monolayers (MLs) reported previously [1]. The diffraction spots have no symmetric counterparts on the opposite side of the The temporal evolution (in the number of deposited MLs) of the integral intensity of 001 diffraction extrapolated to zero thickness indicates a linear growth of the lying-down phase from the very beginning of deposition (Fig. 4a) when the scattered intensity was too low to be measured (yellow region). While the lateral q_{xy} width of 001 diffraction spot is controlled by the limited resolution at grazing incidence, q_z shows an increase in islands height from 25 nm to 44 nm between 2.5 and 8 MLs before the resolution limit is reached (Fig. 4a). The temporal evolution of the islands dimensions evaluated from AFM images taken ex-situ at selected deposition times suggests a strongly asymmetric growth due to the saturation of the islands width and height at 1 ML thickness (Fig. 4b). The asymmetry is driven by different surface energies of (001), (010) and (001) facets (Fig. 2c) that are 3.1, 4.8 and 6.4 meV/Å^2, respectively.

The kinetics of PEN crystals growth was studied by in-situ GISAXS. It could be measured simultaneously with GIWAXS as the in-plane Bragg angle of 001 diffraction was slightly deviated from the graphene zigzag direction (Fig. 2a). Due to the low PEN islands density and large interisland distances exceeding experimental GISAXS resolution, the measured GISAXS curve is primarily controlled by the interplay of three form factors corresponding to three different crystal orientations (Fig. 2c). Hence, it could be evaluated by Guinier analysis. As a consequence of the highly anisotropic crystals growth, these form factors contribute to GISAXS curve in different q ranges. Consequently, Guinier analysis in a q range of $(1\div2)\times10^{-3}$ Å^{-1} allowed to analyze the temporal evolution of the radius of gyration which could be attributed to a half of the islands width (Fig. 5). A fit with a simple exponential

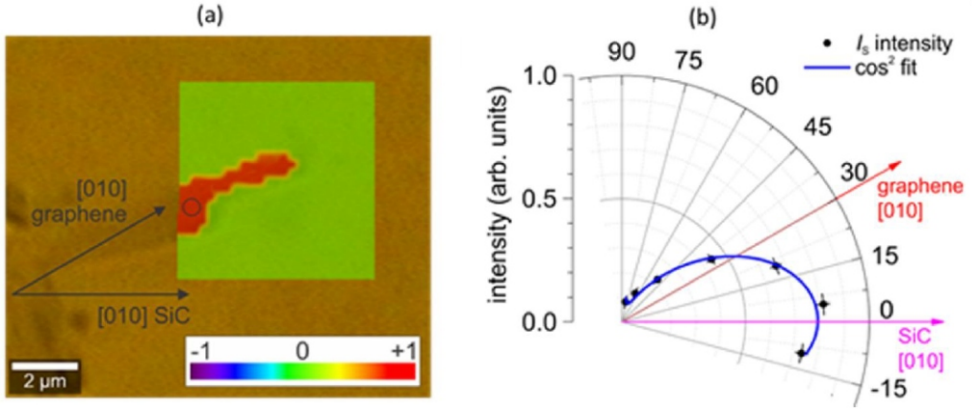

Figure 3. (a) Overlap of the optical and Raman images of a PEN island and (b) $\cos^2$ fit of the azimuthal dependence of Raman band integral intensity at 1373 cm^{-1} (short molecular axis vibrations) inside the black circle in (a).

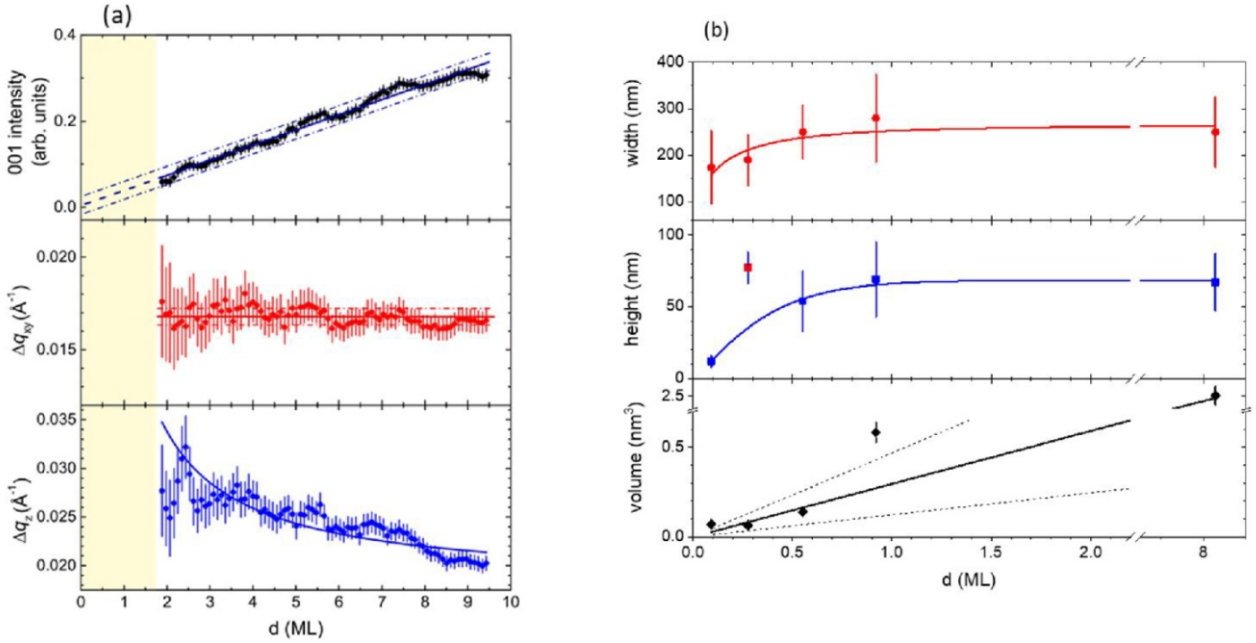

Figure 4. (a) Temporal evolution of PEN 001 diffraction peak parameters and (b) dimensions of PEN islands. (dots - measured points, lines – fits).

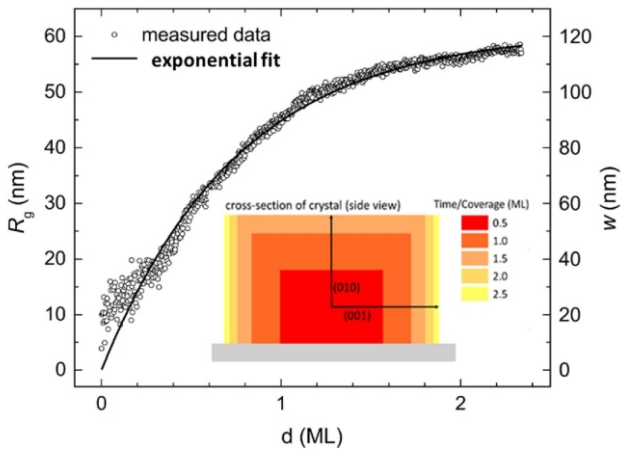

Figure 5. Temporal evolution of the radius of gyration $R_g = " w$ (w – PEN islands width). The inset shows the growth of (100) facets.

limited growth function provided a rate constant of $(3.5 \pm 0.03)\times10^{-3}$ s^{-1}. Combining these results with AFM data, the growth of (100) facets (Fig. 2c) can be visualized (inset in Fig. 5).

Summarizing, a comprehensive time-resolved study of PEN thermal evaporation on a large-area graphene monolayer on SiC revealed a highly anisotropic epitaxial two-stage growth of a laying-down phase in the form of elongated islands following hexagonal symmetry of the substrate. The PEN islands posses triclinic monocrystalline structure, the long molecular axis being deviated from graphene by 11° in the final stage.

1. D. Nabok, P. Puschnig, C. Ambrosch-Draxl, O. Werzer, R. Resel, D.-M. Smilgies, *Phys. Rev. B*, **76**, (2007), 235322.

2. C. C. Mattheus, A. B. Dros, A. J. Baas, A. Meetsma, J. L. de Boer, T. T. M. Palstra, *Acta Crystallogr. C*, **57**, (2001), 939.

The work was done during implementation of the project with ITMS code 26210120023 supported by the Research and Development Operational Programme funded by the ERDF.

L17

X-RAY DIFFRACTION ANALYSIS OF EPITAXIAL LAYERS WITH DEPTH-DEPENDENT COMPOSITION

E. Dobročka

Institute of Electrical Engineering, Slovak Academy of Sciences, Dúbravská cesta 9,841 04 Bratislava, Slovak Republic
edmund.dobrocka@savba.sk

High resolution mode is a special branch of X-ray diffraction techniques devoted to the analysis of single crystalline epitaxial layers. One of the most important tasks in epitaxial technologies is the determination of the layer composition. For epitaxial systems with high degree of perfection, e. g. Si- or GaAs-based compounds, the recorded diffraction curves have rather complex form and the layer parameters are routinely determined by computer simulation of the model structure. For epitaxial layers based on materials with lower quality and/or larger lattice mismatch, the fine features of the diffraction curves are missing and only more or less separated diffraction maxima of individual layers can be observed. Typical examples of such materials are the III–nitride semiconductors as AlN, GaN, InN and their ternary alloys. These materials have great potential for use in optoelectronic and high-temperature electronic devices due to their wide range of bandgaps and high-temperature stability [1-3].

If the layers are perfectly matched to the substrate, it is sufficient the measuring of one symmetric diffraction of the type 000*l*. But in the case of layers exhibiting certain degree of relaxation, in addition to the symmetric diffraction, at least one asymmetric diffraction has to be measured. From the position of the diffraction spots the composition as well as the degree of relaxation can be determined. For the GaN based compounds the most convenient and accessible asymmetric diffraction is $11\bar{2}4$. There are six equivalent diffractions of this type in hexagonal materials but if the lattice tilting does not take place, it is, in principle, sufficient to measure only one of these diffractions. However, measuring of several diffractions increases the precision of the evaluation. Further simplification stems from the symmetry of the stress state of the layer. Hexagonal c-oriented epitaxial layers are transversely isotropic, i.e. the deformation of the layer is completely described by two nonzero strain components:

$$\varepsilon_{\parallel}(x) = \frac{a - a_0(x)}{a_0(x)}, \quad \varepsilon_{\perp}(x) = \frac{c - c_0(x)}{c_0(x)}, \tag{1}$$

where a, c and a_0, c_0 are the lattice parameters of strained (and measured) and fully relaxed layer, respectively [4]. These components are connected by the relation

$$\varepsilon_{\perp} = -2\frac{c_{13}(x)}{c_{33}(x)}\varepsilon_{\parallel}, \tag{2}$$

where $c_{13}(x)$ and $c_{33}(x)$ are the composition dependent stiffness constants of the material. Alternatively, instead of in-plane strain $_{\parallel}$, the degree of relaxation R defined as

$$R = \frac{a - a_{GaN}}{a_0 - a_{GaN}} \tag{3}$$

is often used to describe the strain state of the epitaxial layer. It has to be pointed out that the parameter characterizes the strain state of the layer with respect to the substrate lattice.

The values of a and c can be calculated from the reciprocal co-ordinates h and l of the layer diffraction spot as [5]

$$a = \frac{1}{h}a_{GaN}, \quad c = \frac{4}{l}c_{GaN}. \tag{4}$$

The unknown composition parameter x and the in-plane strain $_{\parallel}(x)$ can be obtained by solving the system of equations in (1) and (2). A simple iterative procedure that uses h and l in (4) as input parameters is outlined in [6]. The method supposes linear dependence of the parameters $a_0(x)$, $c_0(x)$ and $c_{13}(x)$, $c_{33}(x)$ on the composition x.

The complete information on the state of the epitaxial layer can be obtained by measuring the reciprocal space map (RSM) around a suitable asymmetric diffraction. For the later purposes it is reasonable to introduce the presentation of the admissible positions of the layer spots in reciprocal space in dependence of the layer composition and the degree of relaxation. It follows from simple geometrical considerations that in the case of AlGaN/GaN and InGaN/GaN systems the possible positions of the layer diffraction spot are confined to triangular region in the vicinity of GaN diffraction. This area is bounded by the so called relaxation line connecting the AlN or InN layer diffraction spots for fully strained and completely relaxed state [7]. The third vertex of the triangle is the GaN substrate (or buffer layer) diffraction spot. However, for the system InAlN/GaN this area comprises two triangular regions as shown in Fig. 1. This is a consequence of the fact that the lattice parameters of GaN are in between the parameters of InN and AlN lattices. The common vertex of these triangles corresponds to the composition of the $In_xAl_{1-x}N$ for which the layer is perfectly matched to the GaN lattice. It is worth noting that this point in reciprocal space does not coincide with the GaN diffraction spot. This is a general property of hexagonal epitaxial systems and it stems from different values of aspect ratios of $In_xAl_{1-x}N$ and GaN lattice.

If $In_xAl_{1-x}N$ layer is grown on GaN buffer layer in sequence (without breaking the growth after GaN), unintentional Ga-auto-incorporation into $In_xAl_{1-x}N$ layer is an obvious problem, as reported in [8-10]. Sources of Ga could be the deposited Ga-containing-residues on the reactor wall, susceptor or shower head during GaN growth.

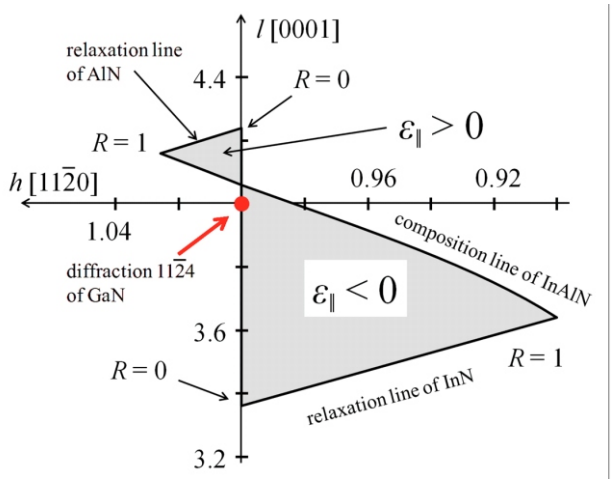

Figure 1. Schematic drawing of the admissible positions of the 11$\bar{2}$4 diffraction spot of InAlN layer for various composition 0 x and degree of relaxation 0 < R < 1. Note the sign of the in-plane strain component $_{\parallel}$ is opposite in Al rich and In rich regions. For the sake of clarity the width of the area is 6-times enlarged.

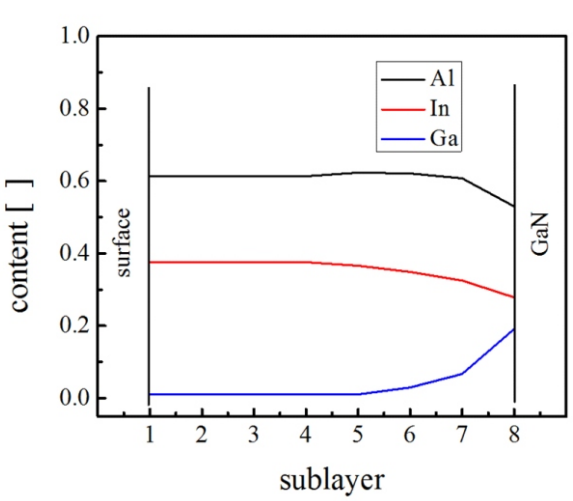

Figure 2. Depth profile of InAlGaN layer composition. The distance between the adjacent sublayers is ~ 40 nm.

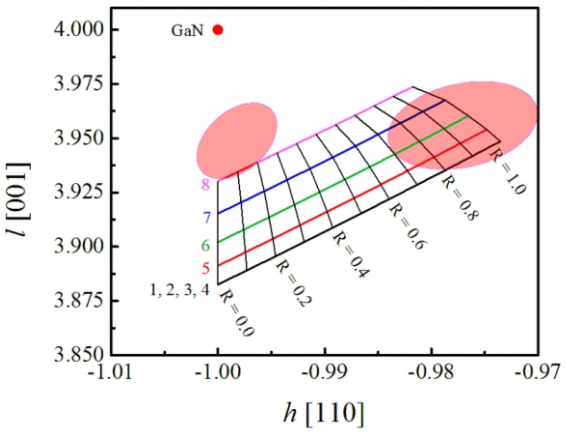

Figure 3. Composition & Relaxation diagram of InAlGaN layer. The position of two maxima revealed by X-ray RSM are schematically shown as ellipses.

Due to the Ga-incorporation in InAlN, intended $In_xAl_{1-x}N$ ternary alloy actually becomes $In_xAl_yGa_{1-x-y}N$ quaternary alloy. This has a significant consequence for the evaluation of X-ray diffraction measurements, e. g. for the interpretation of the RSM. In the case of ternary compounds each couple of lattice parameters a and c of strained layer measured by X-ray diffraction has a unique solution $_{\parallel}$, a_0 , c_0 and x. Evidently, this is not valid for quaternary compounds. In this case the composition of the layer is described by two parameters, e. g. $In_xAl_yGa_{1-x-y}N$, and the measured values of strained lattice parameters a and c can be interpreted by an infinite number of x, y values resulting in different relaxed lattice parameters a_0, c_0 and different degree of in-plane strain $_{\parallel}$. As an illustration, in Tab. 1 five different compositions of quaternary $In_xAl_yGa_{1-x-y}N$ layer resulting in the same values of measured lattice parameters are listed.

This example clearly demonstrates that in the case of quaternary compounds the X-ray measurements alone are insufficient for the determination of the layer composition and further independent analytical technique is required for the evaluation of the structural parameters of the layer. Moreover, the concentration of Ga atoms in the $In_xAl_{1-x}N$ layer is strongly dept-dependent with higher value at the bottom close to the GaN buffer layer. The depth distribution of the elements in the quaternary layer can be determined e. g. by Rutherford backscattering spectrometry (RBS), X-ray photoelectron spectroscopy etc. An example of depth profile of the layer composition obtained by RBS measurement is given in Fig. 2. It is seen that the highest concentration, almost 20%, of Ga is at the bottom of the layer and from the middle up to the layer surface the Ga

Table 1. Five compositions of quaternary $In_xAl_yGa_{1-x-y}N$ layer for the same values of measured lattice parameters and corresponding relaxed lattice parameters a_0, c_0, and in-plane strain component $_{\parallel}$.

Ga [%]	In [%]	Al [%]	a_0 [nm]	c_0 [nm]	$_{\parallel}$ [%]
0.0	18.4	81.6	0.31898	0.51134	- 0.14
5.0	17.2	77.8	0.31884	0.51147	- 0.09
10.0	16.0	74.0	0.31870	0.51160	- 0.05
15.0	14.7	70.3	0.31856	0.51173	- 0.006
20.0	13.5	66.5	0.31843	0.51187	0.04

content is negligible. The distance between the adjacent sublayers is ~ 40 nm. The total layer thickness is ~280 nm. These measurements can be combined with the X-ray results in the way outlined in the following.

The data describing the depth distribution of the elements in the layer are used as input parameters and the theoretical relaxation lines are calculated for all sublayers with their particular composition obtained by RBS analysis. The set of calculated relaxation lines plotted in reciprocal space build up a special mesh – the composition & relaxation diagram. Each relaxation line in this diagram is connected with a sublayer in different depth, hence at favourable circumstances the eventual depth distribution of the relaxation can be established simply by comparison of the diagram with the measured RSM (not shown here). Such a comparison is given in Fig. 3.

It is seen that in addition to the basic GaN diffraction $11\bar{2}4$ two distinct but rather broad maxima corresponding to epitaxial layer were revealed. They are schematically depicted in the diagram as transparent red ellipses. The curves of constant degree of relaxation are also shown. It can be concluded that the InAlN layer with incorporated Ga atoms is apparently divided into two layers. The maximum on the left side can be ascribed to the bottom layer with high Ga content. The layer is almost perfectly matched to the GaN buffer layer. It is also evident that the Ga content provided by RBS measurement is somewhat underestimated, the maximum does not lie on the deepest relaxation line having the highest Ga content. The right side maximum can be related to the upper layer with negligible Ga content. The layer is almost fully relaxed.

1. J. Kuzmík, *IEEE Electron Device Lett.*, **22**, (2001), 510.
2. Y. Yue, Z. Hu, J. Guo, B. Sensale-Rodriguez, G. Li, R. Wang, F. Faria, T. Fang, B. Song, X. Gao, *IEEE Electron Device Lett*., **33**, (2012), 988.
3. J. Kuzmík, A. Georgakilas, *IEEE Trans. Electron Dev*., **58**, (2011), 720.
4. A. Krost, A. Dadgar, G. Strassburger, R. Clos, phys. status solidi A, **200**, (2003), 26.
5. E. Dobročka, S. Hasenöhrl, P. Chauhan, J. Kuzmík, *Appl. Surf. Sci*. **461**, (2018), 23.
6. P. Chauhan, S. Hasenöhrl, E. Dobročka, Ľ. Vančo, R. Stoklas, J. Kováč, P. Šiffalovič, J. Kuzmík, *Appl. Surf. Sci*. **470**, (2019), 1.
7. U. Pietsch, V. Holý, T. Baumbach, *High-Resolution X-Ray Scattering, second ed*., Springer, New York, 2004.
8. S. Choi, H. J. Kim, Z. Lochner, J. Kim, R. D. Dupuis, A. M. Fischer, Yu. R. Juday, T. L. Huang, J. Y. Huang, F. A. Ponce, J.-H. Ryou, *J. Cryst. Growth*, **388**, (2014), 137.
9. J. Kim, Z. Lochner, M.-H. Ji, S. Choi, H. J. Kim, J. S. Kim, R. D. Dupuis, A. M. Fischer, Yu. R. Juday, T. L. Huang, J. Y. Huang, F. A. Ponce, J.-H. Ryou, *J. Cryst. Growth*, **388**, (2014), 143.
10. M. Hiroki, Y. Oda, N. Watanabe, N. Maeda, H. Yokoyama, K. Kumakura, H. Yamamoto, *J. Cryst. Growth*, **382**, (2013), 36.

The author gratefully acknowledges S. Hasenöhrl for providing the sample and D. Machajdík for RBS measurement.

L18

DEVELOPMENT OF X-RAY ANALYTICAL TECHNIQUES USING STANDARD LABORATORY DIFFRACTOMETERS

O. Caha

Department of condensed matter physics, Masaryk University, Kotlářská 2, 611 37 Brno
caha@physics.muni.cz

In the last couple of years our laboratory has implemented couple of X-ray analytical techniques unusual in laboratories. We will present couple of methods which has been implemented and succesfully tested. We will discuss standing wave X-ray fluorescence, rocking curve imaging and absorption spectroscopy.

X-ray fluorescence spectroscopy was implemented using energy dispersive detector Amptek (Si PIN diode). The detector was mounted as the second detector to the standard X-ray diffractometer with copper or molybdenum anode. The primary beam is monochromatized and collimated with a multilayer parabolic Göbel mirror and Ge(220) channel cut monochromator. We have measured angle of incidence dependence of the fluorescence radiation simultaneously with reflected or diffracted radiation. In usual case the method allows us to determine depth profile of the chemical composition. The measurement is usually performed for low angles of incidence; penetration depth changes from couple of nanometers below angle of total external reflection towards couple of micrometers for higher angles of incidence.

As an example we present results obtained at polycrystalline periodic multilayers FeCo/Al_2O_3. The samples have very thin layers of magnetic FeCo with thickness between 1.3 nm to 2 nm separated by 3 nm spacer of insulating Al_2O_3. The samples with thinner FeCo layer exhibit superparamgnetic properties with extremally high relative permeability values up to 10^4. We have studied the samples using X-ray fluorescence and diffraction at low angles of incindence. At the reflection maxima the incident and reflected wave form a standing wave within the superlattice. Fitting angular dependences of fluorescence and diffraction signal we were able to determine size and position of crystalline FeCo particles and also compositional profile of

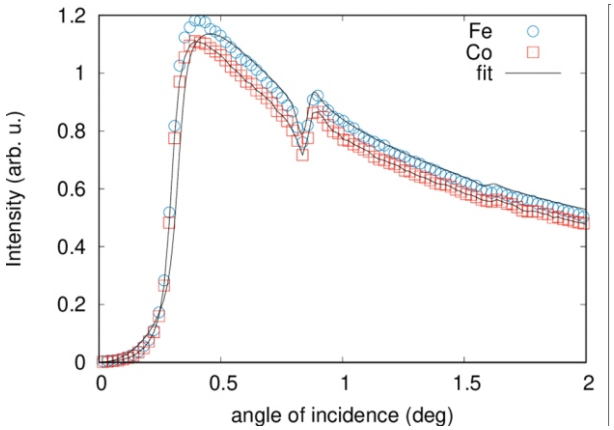

Figure 1. Angle of incidence dependence of Fe and Co fluorescence signal.

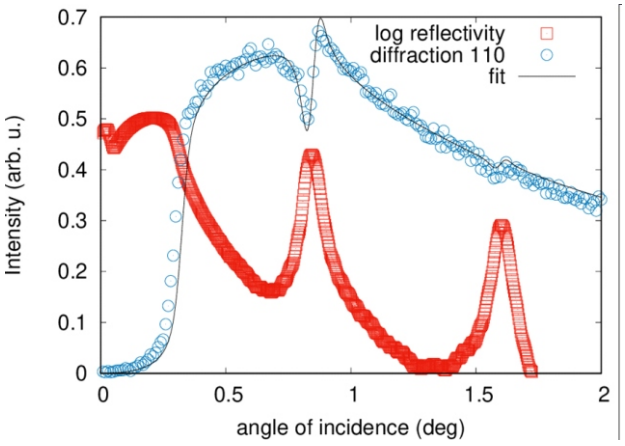

Figure 2. Angle of incidence dependence of FeCo 110 diffraction signal. Reflectivity curve in logaritmic scale.

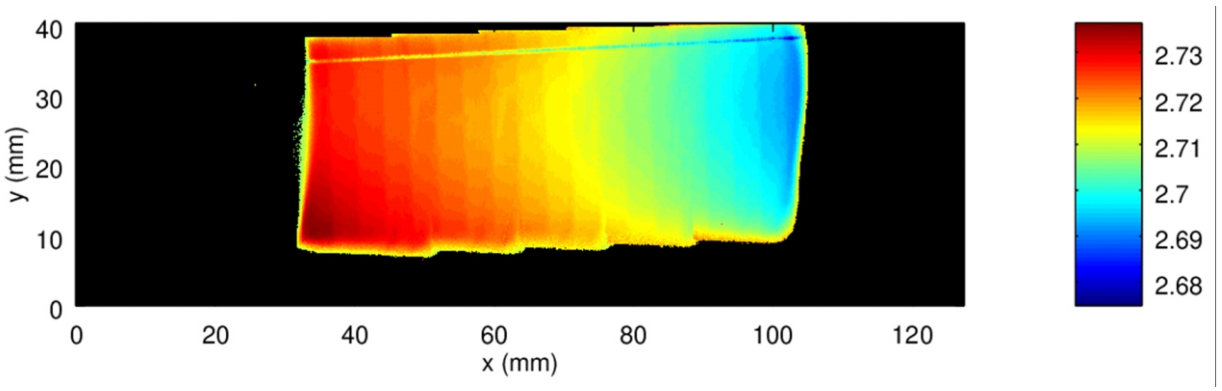

Figure 3. Map of 311 diffraction peak position measured at bent silicon wafer.

Fe and Co in the superlattice. We have found the concentration of interdiffused metallic atoms into insulating spacer to be between 8% and 10% [1]. The examples of fluorescnce and diffraction profiles are presented in figures 1 and 2.

Another method implemented in our laboratory is rocking curve imaging using two dimensional detector. We have used diffractometer Rigaku SmartLab with 2D detector Hypix3000, which we have mouted close to the sample using a home made holder. The detector can be put at the minimal distance of approximately 10 mm from the sample in the case of asymmetric grazing incidence diffraction. Such setup has also advantage of large irradiated area with a limited beam size and low divergence of the diffracted beam. The resolution is limited by the pixel size of detector (0.1x0.1 mm^2). At the angle of incidence of 1° we can achieve irradiated area up to 25x60 mm^2. This method can provide locally resolved informations such as curvature of the sample, chemical composition of alloyed layers, diffraction peak width and intensities, which present information of defects. The example of the peak position map of bent silicon wafer is presented in figure 3.

Last presented method is x-ray absorption spectroscopy used for absolute quantification of certain elements concetration. We have used it for barium quantification in a medical radiation shielding foil. We have again used standard x-ray diffractometer with copper rotating anode and accelerating voltage of 45 kV. The barium K absorption edge (38 keV) was then measured with a white primary beam in Bragg-Brentano setup monochromatized with a silicon (111) monocrystal. Measurement in tha Bragg angle range of 5° to 7° corresponds to energy range 44 to 33 keV. This range covers clearly barium absorption edge allowing us to determine absolute concentration usin tabulated values of absorption coefficients [2].

1. C. V. Falub, S. V. Pietambaram, O. Yildirim, M. Meduňa, O. Caha, R. Hida, X. Zhao, J. Ambrosini, H. Rohrmann, and H. J. Hug, *AIP Advances*, **9**, (2019), 035243.

2. S. Brennan, P. L. Cowan, *Review of Scientific Instruments*, **63**, (1992), 850.

L19

IMPACT OF SUBSTRATE ON PREFERENTIAL ORIENTATION OF NbN THIN LAYERS

T. Roch[1], S. Volkov[1], M. Gregor[1], L. Satrapinskyy[1], T. Fiantok[1], M. Čaplovičová[2]

[1]Department of Experimental Physics, Faculty of Mathematics Physics and Informatics, Comenius University in Bratislava, Mlynska Dolina, 842 48 Bratislava, Slovakia

[2]Slovak University of Technology in Bratislava, University Science Park Bratislava Centre, Vazovova 5, 812 43 Bratislava, Slovak Republic

roch@fmph.uniba.sk

Relatively simple NbN superconducting and protective coating material is still attractive due to its superconductive critical transition temperature T_c around 16K, the critical current density j_c for thin films in the order of several MA/cm^2 and very high critical magnetic fields of up to 40T [1]. Typically the best superconducting properties are obtained in epitaxially grown cubic NbN on MgO substrate with misfit value of 4.3%. Recently we have prepared thin highly oriented NbN layers on Si, MgO, and Al_2O_3 substrates [2].

In present work we have investigated in more detail structural properties of NbN epitaxial layers deposited on various substrates. Nitride layers were deposited on heated substrates by pulsed laser ablation from Nb target in Ar : N gas mixture. Technological conditions have been chosen in order to obtain highly oriented – epitaxial fcc-NbN thin films. Surprisingly, although the nominal misfit of NbN on c-cut sapphire substrate is 13.1%, it showed highest T_c = 16.4 K in comparison to sample on MgO (T_c = 13.1 K) and Si (T_c = 8.3 K). When assuming domain epitaxy: ($8d_{NbN} - 9d_{Al2O3}$)/ $9d_{Al2O3}$, the effective mismatch can be decreased to 0.5% [3].

The XRD analysis involved determination of the relaxation status and coherent blocks dimensions by reciprocal space mapping and texture investigation by pole figures measurement. Surface topography has been characterized by atomic force microscopy and the local structure around substrate interface using high resolution transmission electron microscopy. Samples on MgO showed typical cube on cube epitaxial relationship NbN(001)[100] || MgO(001)[100], whereas samples on c-cut sapphire: NbN(111)[$1\bar{1}0$] || Al_2O_3(0001)[$10\bar{1}0$] (Fig.1). For the case of r-cut Al_2O_3 substrate the pole figures measured at 111NbN showed that the films are twinned and strongly oriented: NbN(135) || Al_2O_3($10\bar{1}2$) (Fig.2).

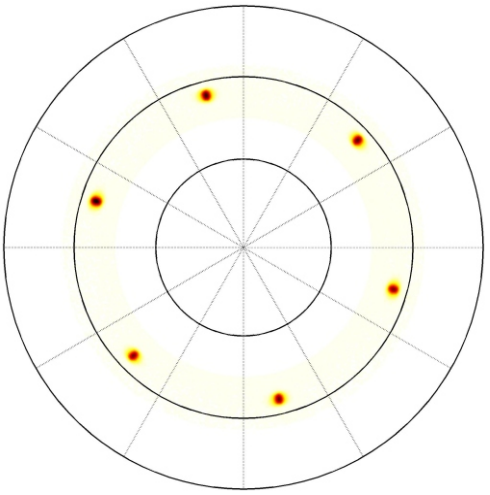

Figure 1. Pole figure in 200 NbN /c-cut Al_2O_3

1. A.D. Pogrebnjak, V.M. Rogoz, O.V. Bondar, N.K. Erdybaeva, S.V. Plotnikov, *Protection of Metals and Physical Chemistry of Surfaces*, **52**, (2016), 802.
2. S. Volkov, M. Gregor, T. Roch, L. Satrapinskyy, B. Grančič, T. Fiantok, A. Plecenik, *J. Electrical Engineering*, (submitted 2019).
3. F. Mercier, S. Coindeau, S.Lay, A. Crisci, M. Benz, T. Encinas, R. Boichot, A. Mantoux, C. Jimenez, F. Weiss, E. Blonquet, *Surface and Coatings Technology*, **260**, (2014), 126.

Authors would like to acknowledge a support by the Slovak Research & Development Agency under contract no. APVV-16-0315.

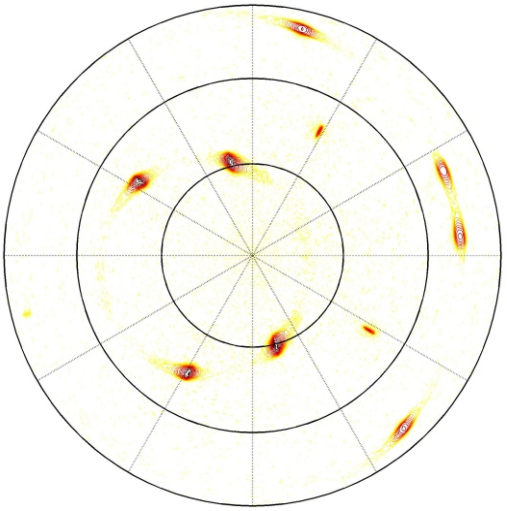

Figure 2. Pole figure in 111 NbN / r-cut Al_2O_3.

L20

HYBRID MULTIPLE DIFFRACTION

E. de Prado[1], J. Kub[1], O. Pacherova[1], A. Hospodková[2], V. Novák[2], M. Cukr[2]

[1]Institute of Physics of the Czech Academy of Sciences, v. v. i., Na Slovance 1999/2, 182 21 Praha 8, Czech Republic
[2]Institute of Physics of the Czech Academy of Sciences, v. v. i., Cukrovarnická 10, 16200 Praha 6, Czech Republic
prado@fzu.cz

The analysis of multiple diffraction (MD) processes could provide an alternative method for the structural characterization of samples. One of the first studies reported on this topic was made by Renninger in 1937 [1] and used for the 222 reflection of diamond, obtaining accurately its lattice parameters [2]. MD takes place inside a material when more than one set of planes fulfills simultaneously the Bragg condition in the path of the incident beam. In the real space it means that a specific diffraction (called primary) can be produced by the combined diffracting effects from two or more different set of planes (Fig. 1). This is possible because the sum of two or more diffraction vectors always end up at a reciprocal-lattice point of their corresponding space. Experimentally, since it is not possible to discriminate the different contributions to diffraction between conventional two-beam diffraction and MD, this phenomenon is generally studied for forbidden or very weak reflections, in which changes in intensity may be more easily observed.

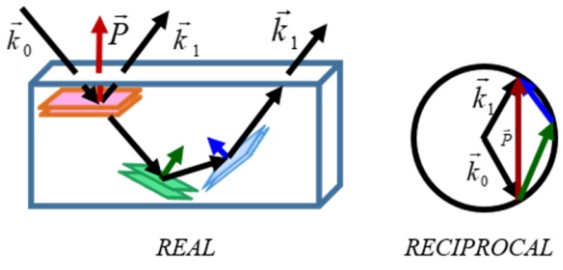

Figure 1. Geometry of a three-beam MD in real and reciprocal space.

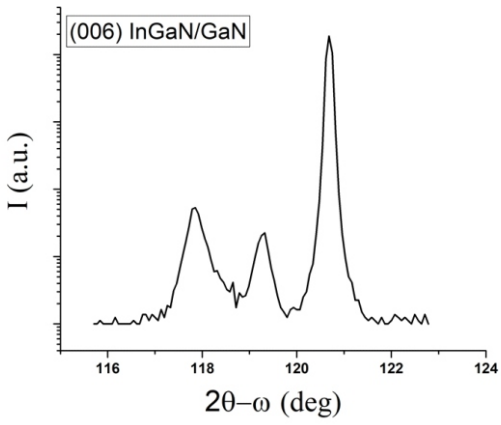

Figure 2. Diffractogram showing the (006) InGaN and GaN reflections and an hybrid peak

Hybrid Multiple Diffraction (HMD) is a particular and poorly studied kind of multiple diffraction that can happen in heteroepitaxial systems. In these systems two different materials are involved in the generation of MD in such a way that the participant planes belong to different reciprocal lattices. In this respect, the final beam is not diffracted exactly towards the outgoing primary direction ( ) but in a direction very close to it (H). Thus HMD phenomenon can be observed also for allowed reflections unlike as happens with MD. One of the first studies in this frame was performed by Isherwood et al. [3], who investigated cubic Ga1-xAlxAs epitaxially grown on (001) GaAs substrates.

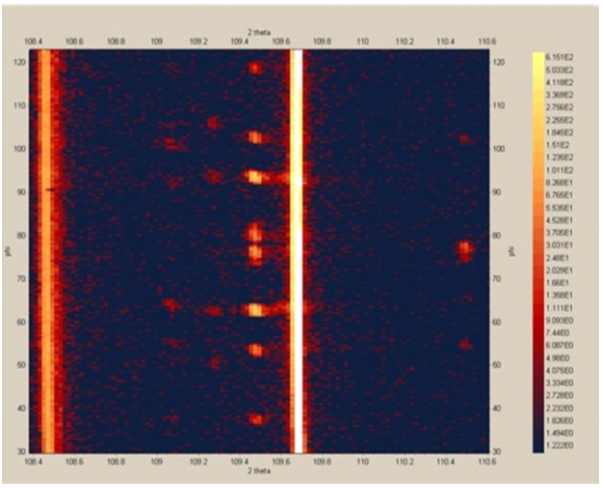

Figure 3. Azimuthal scan around (006) symmetric reflection showing the signal from the layer, the substrate and the hybrid points

Later, it was studied by Morelhao *et al*. [4-8] and Domagala and coworkers for different cubic and, ultimately, for wurtzite *c*-oriented materials [9] and by E. de Prado *et al* [10] for *r*-oriented wurtzite structures.

The three-beam X-Ray diffraction condition can be fulfilled by rotating the sample around the primary diffraction vector **P** of the reflection whose intensity is monitored, generally a symmetric one. That is, participant planes are excited only at some specific azimuthal angles of the incident direction. This makes that this type of diffraction could be observed only for some particular azimuthal angles.

In this work we show some additional conditions that must been satisfied in order to achieve HMD. To illustrate it we present our study on an InGaN thin layer grown by Metal Organic Vapor Phase Epitaxy (MOVPE) on a thick GaN buffered *c*-Al_2O_3 substrate (Fig 2).

We present also an easy procedure for identify the participant planes in the HMD process using for that a thick MnGaAs layer grown by Molecular Beam Epitaxy on GaAs c-oriented substrate. In this sample all the hybrid reflections (Fig 3) were identified.

1. M. Renninger, "'Detour-excitation' a hitherto unobserved interaction effect in space-lattice interference," *Zeitschrift für Phys*., vol. 106, no. November, pp. 141–76, 1937.
2. M. Renninger, "Beitrag zur Kenntnis der röntgenographischen Unterschiede zwischen den beiden Diamant-Typen," *Acta Crystallogr.*, vol. 8, no. 10, pp. 606–610, 1955.
3. B. J. Isherwood, B. R. Brown, and M. A. G. Halliwell, "X-ray multiple diffraction as a tool for studying heteroepitaxial layers. I. Coherent, on-axis layers," *J. Cryst. Growth*, vol. 54, no. 3, pp. 449–460, 1981.
4. S. L. Morelhão and L. P. Cardoso, "Simulation of hybrid reflections in X-ray multiple diffraction experiments," *J. Cryst. Growth*, vol. 110, no. 3, pp. 543–552, 1991.
5. S. L. Morelhão, L. P. Cardoso, J. M. Sasaki, and M. M. G. De Carvalho, "Hybrid multiple diffraction in Renninger scan for heteroepitaxial layers," *J. Appl. Phys.*, vol. 70, no. 5, pp. 2589–2593, 1991.
6. S. L. Morelhão and L. P. Cardoso, "Structural properties of heteroepitaxial systems using hybrid multiple diffraction in Renninger scans," *J. Appl. Phys.*, vol. 73, no. 9, pp. 4218–4226, 1993.
7. S. L. Morelhão, A. A. Quivy, and J. Härtwig, "Hybrid and effective satellites for studying superlattices," *Microelectronics J.*, vol. 34, no. 5–8, pp. 695–699, 2003.
8. S. L. Morelhão and J. Z. Domagala, "Hybrid reciprocal space for X-ray diffraction in epitaxic layers," *J. Appl. Crystallogr*., vol. 40, no. 3, pp. 546–551, 2007.
9. J. Z. Domagala, S. L. Morelhão, M. Sarzynski, M. Mazdziarz, P. Dluzewski, and M. Leszczynski, "Hybrid reciprocal lattice: application to layer stress appointment in GaAlN/GaN(0001) systems with patterned substrates," *J. Appl. Crystallogr.*, vol. 49, no. June, pp. 798–805, 2016.
10. E. De Prado, M. C. Martinez-Tomas, C. Deparis, V. Munoz-Sanjose, and J. Zuniga-Perezb, "Hybrid multiple diffraction in semipolar wurtzite materials: (0112)-oriented ZnMgO/ZnO heterostructures as an illustration," *J. Appl. Crystallogr*., vol. 50, pp. 1165–1173, 2017.